JOURNAL OF GUIDANCE, CONTROL, AND DYNAMICS
Vol. 31, No. 4, July–August 2008

Optimization of Perching Maneuvers Through Vehicle Morphing

Adam M. Wickenheiser* and Ephrahim Garcia†
Cornell University, Ithaca, New York 14850

DOI: 10.2514/1.33819

This paper discusses the development and optimization of trajectories designed to bring a long endurance unmanned aerial vehicle from a loitering state to a planted landing referred to as a perching maneuver. These trajectories are developed for attached, partially stalled, and fully stalled flow regimes. The effects of nonlinear aerodynamics and vehicle shape reconfiguration are shown to lessen the initial distance from the landing site required to initiate the maneuver, reduce the spatial bounds on the trajectory, and decrease the required thrust for the maneuver. The aerodynamics are modeled using empirical and analytical methods in both attached and separated flow regimes. Optimal solutions of varying thrust-to-weight ratio and center-of-gravity location are compared. Additionally, perching trajectories that compare morphing versus fixed configuration and stalled versus unstalled aircraft are presented to demonstrate the effects of relaxed constraints on vehicle geometry and flight envelope. Control effort is also evaluated in these simulations; specifically, the available control for disturbance rejection is compared for morphing versus fixed-configuration aircraft. The results of these comparisons show that morphing increases the controllability of the aircraft throughout the maneuver as well as decreases the cost of the optimal perching trajectory.

Nomenclature

C_D	=	drag coefficient
C_d	=	section drag coefficient
C_L	=	lift coefficient
C_l	=	section lift coefficient
C_M	=	pitch moment coefficient
c	=	local chord length
$\bar{c}$	=	mean aerodynamic chord
g	=	acceleration due to gravity
h	=	vertical position
I_y	=	principal moment of inertia about pitch axis
J	=	cost function
l	=	characteristic length
m	=	aircraft mass
p	=	dynamic mixing parameter
p_0	=	static mixing parameter
q	=	pitch rate
S	=	planform area
T	=	thrust magnitude
T/W	=	thrust-to-weight ratio
t	=	time
V	=	aircraft velocity magnitude
$\mathbf{x}$	=	aircraft longitudinal state vector
x	=	horizontal position
x_{cg}	=	aircraft center of gravity
x_{cp}	=	airfoil center of pressure
x_{np}	=	aircraft neutral point
α	=	angle of attack
γ	=	flight path angle
δ_e	=	elevator deflection angle
θ	=	pitch angle
θ_b	=	tail boom angle with respect to fuselage
θ_t	=	tail angle with respect to boom
ι	=	wing incidence angle with respect to fuselage
κ	=	pitch moment scaling factor
ρ	=	air density
τ_1, τ_2	=	time constants

Subscripts

att	=	attached flow regime
climb	=	climb phase
dive	=	dive phase
f	=	final
fuse	=	fuselage lifting surface
sep	=	separated flow regime
tail	=	tail lifting surface
wing	=	wing lifting surfaces
0	=	initial

Received 2 August 2007; revision received 2 January 2008; accepted for publication 8 January 2008.

*Graduate Student, Sibley School of Mechanical and Aerospace Engineering, 226 Upson Hall. Student Member AIAA.

†Associate Professor, Sibley School of Mechanical and Aerospace Engineering, 224 Upson Hall. Member AIAA.

I. Introduction

LATELY, advances in smart materials, actuators, and control systems have enabled the development of new capabilities for aircraft [1]. Several studies have indicated that gross airframe reconfiguration in particular can lead to increased flight performance and mission potential [2–4]. These studies have shown that in-flight vehicle morphing can grant a single aircraft increased performance by several typically incompatible metrics such as endurance, turn radius, and dash speed. Traditionally, aircraft reconfiguration has been limited to discrete control surfaces such as flaps and slats or variable-swept wings, such as those on the F-14 or B-1 aircraft; however, recent programs have been focused on more radical shape changes. For example, Lockheed Martin Skunkworks [5] and NextGen Aeronautics [6] have each produced flight-tested morphing unmanned aerial vehicles (UAVs) that address the problem of adding dash capabilities to intelligence, surveillance, and reconnaissance (ISR) platforms. The primary hurdle is that long endurance aircraft typically have high aspect ratio wings to increase lift-to-drag efficiency, whereas strike aircraft have shorter delta wings for improved high-speed flight. Both morphing UAVs use segmented folding wing mechanisms, the former a gull-like wing and the latter a batlike wing, to reduce the planform area and span of the wing drastically, thereby enabling high endurance and dash capabilities on a single airframe. In addition, new research has focused on developing bioinspired

flight capabilities for man-made aircraft, including flapping wing flight [7]. Characterizations of this complex flight mechanism have come from experimental data, both insect [8] and avian [9], and computational fluid dynamics [10].

Another bioinspired maneuver under development is perching. Perching can be described as a high angle-of-attack approach with the purpose of using high-drag, separated flow for braking, followed by a planted landing [11,12]. Whereas vertical landings are relatively straightforward for high thrust-to-weight aircraft, it has yet to be demonstrated for high-efficiency reconnaissance platforms. For example, the perching capability could enable an ISR mission length to be extended dramatically: once a target has been found, the aircraft may land on a nearby structure and continue to survey an area without consuming fuel for flight. Depending on the size and weight of the aircraft, this structure could assume a variety of forms in an urban or natural environment, such as a building ledge, power line, cliff side, or tree branch. It is for this reason that the development of practical perching maneuvers for low thrust-to-weight aircraft is the focus of this paper.

ISR aircraft generally do not feature high thrust or thrust vectoring; therefore, another mechanism for decelerating the vehicle must be exploited. In addition, the stall speed of low-thrust aircraft is usually too high for landing on a small surface. Akin to soaring birds [13], a perching aircraft of low thrust-to-weight ratio must fly below the point of landing and then "pop up" just before touchdown, using gravity to drain away the last of its kinetic energy. Although this undershoot is impossible on flat ground, it can be exploited for a short landing on an elevated platform. In an urban environment, this type of landing site is prevalent and is ideal for extended surveillance missions, as previously mentioned. To generate the most rapid decrease in kinetic energy, flying in a stalled flow regime is desirable; however, this introduces stability and controllability problems because unsteady force amplitudes from the separated wake are high and the effectiveness of control surfaces is greatly diminished.

Aerodynamic perching has been studied before in the form of stalled landings of conventional airframes [14]; however, the controllability of a typical low-thrust aircraft in a deep stall is questionable, and the large undershoot of the trajectory relative to the landing site is undesirable. In the present work, it is proposed that in-flight shape reconfiguration will be able to alleviate both of these concerns. This study expands upon the previous work by considering shape changing aircraft with varying constraints on the actuators and optimizing the overall trajectory in addition to just the terminal condition, as discussed next.

The particular aircraft used to develop the perching maneuver is based on the Aerial Regional-Scale Environmental Survey (ARES) Mars scout craft, an aircraft designed to unfold from a Viking derivative aeroshell and fly for approximately 81 min over a Martian landscape, collecting data on atmospheric chemistry, geology, and crustal magnetism [15]. The complete details of the perching aircraft's capabilities are described in [12]; however, the prominent features are depicted in Fig. 1. Unlike the original ARES or any conventional aircraft, additional degrees of freedom are incorporated into the tail boom and tail incidence, and variable incidence is added to the wing sections (or outboard sections of the blended wing body). These degrees of freedom allow the aircraft to change shape in flight, thus grossly altering the geometry and the aerodynamics of the aircraft. In addition, the airfoils are modified for flight in Earth's atmosphere, and the inverted V tail in the original ARES is converted to a standard V tail to protect the structure on hard landings. Previous work [12] has analyzed the open-loop stability and transient response to changing shape configurations and has shown that the proposed morphing scheme is a useful means of reducing the aircraft's speed while maintaining greater control effectiveness than a simple "pitch-up" maneuver.

The principal reasoning behind these additional degrees of freedom is to create regions of attached and separated flow over the aircraft through various flight regimes, as depicted in Fig. 2. To be demonstrated, high-drag, separated flows are necessary to produce practical perching maneuvers. However, it is also desired to maintain controllability about the aircraft's axes of rotation, for which attached flow over the control surfaces is necessary. Thus, whereas the fuselage (or inboard section of the blended wing body) is pitched up to high incidence, the wings are rotated down to maintain attached flow over the ailerons. Additionally, the tail is rotated down and out of the resulting unsteady wake of the body, and the horizontal stabilizer is also actuated to keep the tail surface horizontal as the tail boom rotates. This morphological change keeps the standard aileron and ruddervator surfaces effective at trimming and control. They also allow a larger degree of control over the aircraft's dynamics through a wider range of flight conditions.

The "direct shooting method" [16] of solving optimization problems is used to convert the nonlinear optimization problem into an equivalent nonlinear programming problem. This procedure involves converting the control time histories into a simple functional form that can be parameterized by a (relatively) small number of constants. Several parameterizations have been tested before selecting a piecewise cubic Hermite interpolation. This method of interpolation can be designed to preserve the monotonicity and extrema of the underlying data [17] as well as providing continuity and continuous differentiability of the time series. This is especially significant because the optimal control strategies tend to be only piecewise continuous due to constraints, which might be violated by any overshoot in the interpolating polynomial. The nonlinear programming method used in this study is a sequence of simulated annealing [18] and sequential quadratic programming [19]. These methods are used together to balance robustness against local minima and speed of convergence. Several methods for discretizing and numerically integrating the dynamics have been considered; however, Matlab's fourth- to fifth-order adaptive Runge–Kutta algorithm [20] has been chosen for its robustness in the face of fast dynamics (i.e., pitch dynamics) coupled with slow dynamics (i.e., translational dynamics).

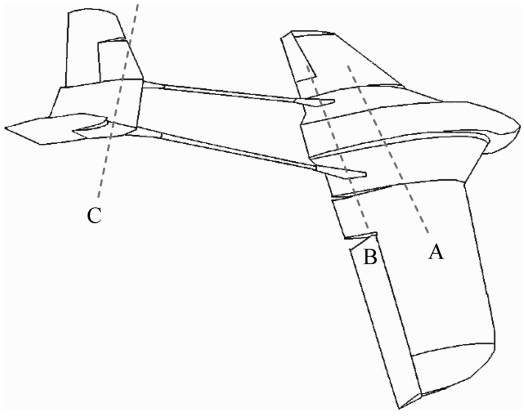

Fig. 1 The three shape-change actuations about the pitch axis: A) rotation of the wing incidence angle with respect to the fuselage body axis, B) rotation of the tail boom, and C) rotation of the horizontal stabilizer.

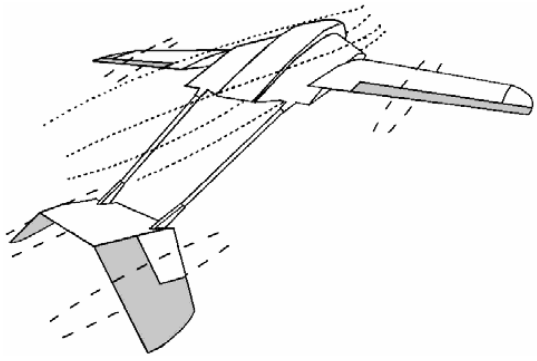

Fig. 2 Regions of attached flow (dashed) and separated flow (dotted) over the aircraft and its control surfaces (shaded) at high angles of attack, after reconfiguration.

In this paper, the perching trajectory optimization problem is rigorously formulated to provide a framework for generating practical maneuvers for the reconnaissance mission previously described, which means reducing the spatial requirements of the trajectory while respecting the capabilities of the aircraft. The governing dynamics of the aircraft and the surrounding flow are presented, as well as the physical and heuristic constraints placed on the solution. This work expands upon the results presented in [21], in which a point-mass aircraft is simulated in a perching maneuver. This paper presents results of the optimization procedure for both fixed-configuration and morphing airframes and compares them to the previous point-mass data. Finally, several conclusions are offered about the important parameters in this problem and about the variations in optimal solutions among these classes of aircraft models.

II. Modeling Description and Problem Formulation

A. Vehicle Model

The aircraft used in this study is modeled as a blended wing body with rotating outboard wing sections, attached via rotating tail booms to a V tail, as depicted in Fig. 1. All of the aircraft controls (standard and morphing) are limited in range and actuation rate, as summarized in Table 1. (The layout of these controls is depicted in [11] and Fig. 3). The lower bound on the tail boom angle is set at −15 deg to keep it out of the unsteady wake behind the fuselage at high angles of attack. For this study, the thrust vector is assumed to be aligned with the chord line of the fuselage, and results are compared for various maximum thrust-to-weight ratios. The nominal values listed in Table 1 correspond to the cruise configuration of the aircraft. The mass and geometry parameters of the baseline aircraft are given in Table 2. The moment of inertia data that are presented are given about the centers of mass of each component; the parallel axis theorem is then used to compute the moments about the hinge locations.

Because the available aerodynamic data presented in the following subsection is limited to the longitudinal plane, the equations of motion must also be restricted to the longitudinal plane. Because the aircraft remains bilaterally symmetric for any morphing configuration, and the ruddervators are only used symmetrically, the aircraft remains in the longitudinal plane in the absence of out-of-plane forces or moments. Thus, this analysis ignores the effects of wind disturbances and asymmetries in the aircraft layout. This simplification still yields the optimal trajectory under the stipulation that all disturbances and modeling errors are zero mean and small compared with the nonlinearities so that they may be modeled as additive perturbation terms [22]. These restrictions also constrain the candidate trajectories to the longitudinal plane. This constraint makes practical sense because longitudinal maneuvers are easier to implement, and heading angle adjustments can be handled by a separate controller.

To maximize the convergence rate and minimize any numerical errors from poor scaling [23], the longitudinal equations of motion are converted into the following nondimensional form:

$$\dot{V} = T\cos\alpha - C_D V^2 - \sin\gamma \tag{1}$$

$$\dot{\gamma} = \frac{T}{V}\sin\alpha + C_L V - \frac{\cos\gamma}{V} \tag{2}$$

Table 1 Actuator constraints

		Nominal value, deg	Range, deg	Maximum rate, deg/s
ι	Wing incidence angle	0	−90–90	±20
θ_b	Tail boom angle	−15	−15–90	±20
θ_t	Tail incidence angle	−15	−90–90	±20
δ_e	Elevator angle	0	−20–20	±40

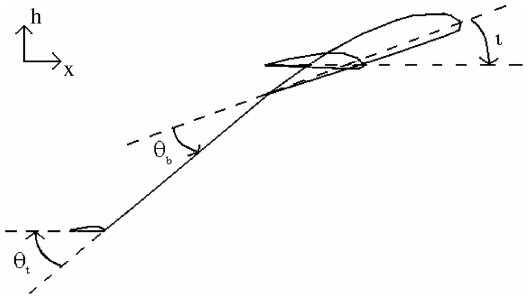

Fig. 3 Morphing parameters, with directions of increasing value.

$$\dot{q} = (\kappa C_M V^2 - \dot{I}_Y q)/I_Y, \qquad \kappa = \frac{2\bar{c}m^2}{\rho S} \tag{3}$$

$$\dot{\theta} = q \tag{4}$$

$$\dot{x} = V\cos\gamma \tag{5}$$

$$\dot{h} = V\sin\gamma \tag{6}$$

$$\alpha = \theta - \gamma \tag{7}$$

where V is in units of $\sqrt{gl}$, t is in units of $\sqrt{g/l}$, T is in units of mg, and x and h are in units of l, where $l = 2m/\rho S$ is the characteristic length. With angles measured in radians, all of the aircraft's states are now of order 1. The aircraft moment of inertia is updated as it morphs, and internal torques are balanced to determine the motion of each component. Although the dynamics of the actuators themselves are not modeled, they are considered fast enough to track the commanded inputs given the constraints listed in Table 1.

B. Aerodynamics

For the purposes of this study, the aircraft is modeled in the longitudinal plane only; that is, roll, yaw, and sideslip dynamics are not considered. This assumption simplifies the aerodynamics and vehicle dynamics substantially while still providing an environment for studying the richness and qualitative behavior of the perching maneuver. The aerodynamic forces on the aircraft components in the attached flow regime are calculated using a modified version of Weissinger's method [24], as developed by Wickenheiser and Garcia [25]. This method is based on classical lifting-line techniques that are

Table 2 Aircraft mass and geometry parameters

Fuselage:			
m	Mass	7.95	kg
I_y	Moment of inertia	0.84	kg · m^2
b	Span	0.81	m
$\bar{c}$	Mean aerodynamic chord	0.69	m
x_{np}	Neutral point (from tip)	0.70	m
Wing:			
m	Mass	1.51	kg
I_y	Moment of inertia	0.02	kg · m^2
b	Span	2.64	m
$\bar{c}$	Mean aerodynamic chord	0.38	m
Tail:			
m	Mass	1.88	kg
I_y	Moment of inertia	0.02	kg · m^2
b	Span (tip to tip)	1.26	m
$\bar{c}$	Mean aerodynamic chord	0.25	m
Γ	Dihedral angle	45	deg
l_{boom}	Boom length	0.79	m

derived from potential flow theory; however, corrections are made to account for experimental airfoil data. This approach has been developed with morphing aircraft in mind; hence, thousands of aircraft configurations have been able to be computed in a matter of days. This process has produced a lookup table of aerodynamics to be used for simulation in the attached flow regime.

Because experimental data of this particular aircraft at high angles of attack are not yet available, flat-plate assumptions and preexisting high angle-of-attack data [26] have been used where the flow is separated. These assumptions are not unreasonable because specific airfoil shape becomes less significant after the flow has detached, as shown experimentally in [26]. The aerodynamic model for fully separated flow is summarized in the following equations:

$$C_{l,\text{sep}} = 1.1\sin(2\alpha) \tag{8}$$

$$C_{d,\text{sep}} = 0.9[1-\cos(2\alpha)] \tag{9}$$

$$\left(\frac{x_{\text{cp}}}{c}\right)_{\text{sep}} = 0.04095\alpha + 0.0857 \tag{10}$$

where the center of pressure in Eq. (10) is measured aft of the quarter-chord point. These section coefficients are then integrated over the wing and tail planforms where the flow is separated. Furthermore, a mixing parameter p is introduced to handle the nonlinear transition between attached and separated aerodynamics and to account for dynamic stall effects. This term is modeled as a first-order lag state, as recommended by Goman and Khrabrov [27], subject to the dynamics of Eq. (11),

$$\tau_1\dot{p} = p_0(\alpha - \tau_2\dot{\alpha}) - p \tag{11}$$

where p_0 is the steady-state mixing function given by

$$p_0(\alpha) = \begin{cases} 1 & |\alpha| < 4 \text{ deg} \\ -0.3326\tan^{-1}\left(\frac{180}{\pi}|\alpha| - 16\right) + 0.5 & 4 \text{ deg} \le |\alpha| \le 37 \text{ deg} \\ 0 & |\alpha| > 37 \text{ deg} \end{cases} \tag{12}$$

Thus, as evinced by Eq. (12) and Fig. 4, $p = 1$ corresponds to fully attached flow, and $p = 0$ corresponds to fully separated flow, with values in between indicating partially separated flows. The model for the mixing parameter given by Eqs. (11) and (12) realistically accounts for static and dynamic stall effects. The $(\alpha - \tau_2\dot{\alpha})$ term accounts for time delays in flow separation and reattachment caused by boundary-layer convection lag, which is roughly proportional to $\dot{\alpha}$. The $\tau_1\dot{p}$ term accounts for the transient response of the flow to disturbances; this is simply modeled as a first-order dynamical system. Both time constants $\tau_{1,2}$ scale with the characteristic time scale $(\bar{c}/V)$. By using the mixing parameter, the lift coefficient for any angle of attack is given by

$$C_L(\alpha,\dot{\alpha}) = C_{L,\text{att}}(\alpha)\cdot p(\alpha,\dot{\alpha}) + C_{L,\text{sep}}(\alpha)\cdot[1 - p(\alpha,\dot{\alpha})] \tag{13}$$

where it is clear that the total force is the weighted sum of the contributions from attached and separated flows. Similar expressions can be written for the drag and pitching moment coefficients. Because the wing and tail incidences can be varied with respect to the fuselage angle of attack, separate states are required to model the degree of separation over each of these surfaces. Thus, the full state vector is

$$\mathbf{x} = [\,V \quad \gamma \quad q \quad \theta \quad x \quad h \quad p_{\text{fuse}} \quad p_{\text{wing}} \quad p_{\text{tail}}\,]^{\text{T}} \tag{14}$$

concatenating states from the equations of motion [Eqs. (1–7)] and the equation of flow separation [Eq. (11)].

In Fig. 5, static C_L and C_M are plotted versus angle of attack for several values of elevator deflection. In the attached flow region, C_L and C_M are approximately linear with respect to angle of attack at each morphing configuration, and the negative C_M slope indicates static pitch stability. At stall, lift decreases rapidly over the aircraft, and the restoring moments begin to level out. This means that less control effort is required to pitch the aircraft further than if the flow had remained attached at all angles. In the next section, the relationship between stability and control effort in the perching

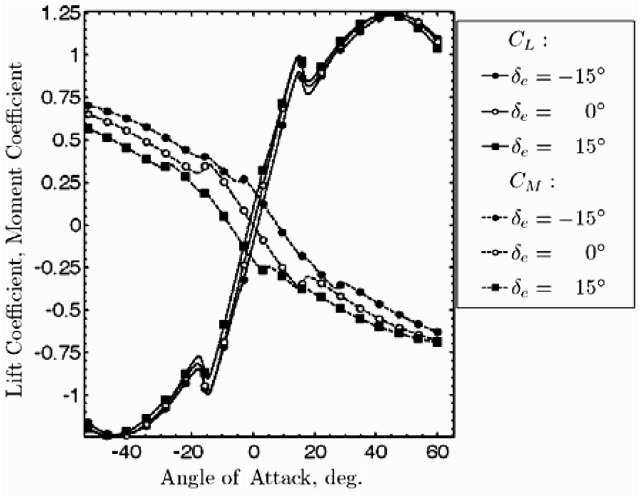

Fig. 5 Lift and moment coefficients for several elevator deflections.

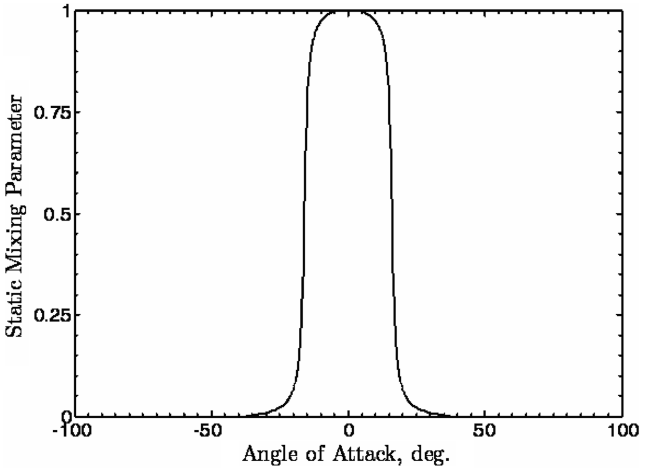

Fig. 4 Static mixing parameter p_0.

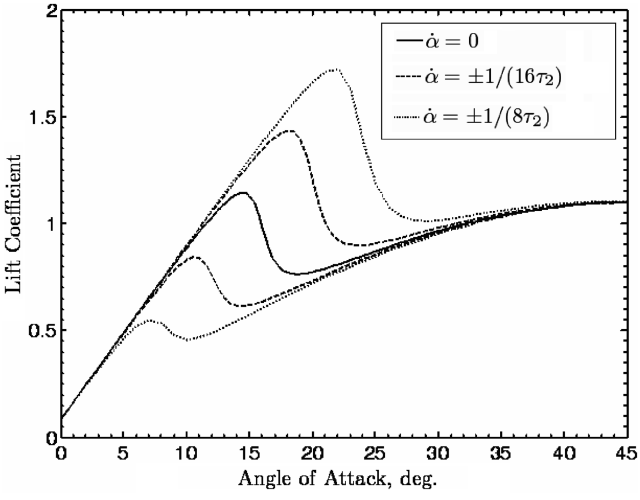

Fig. 6 Dynamic stall due to rapid angle-of-attack changes.

maneuver is discussed in detail, especially with regards to the cost being optimized. Figure 6 depicts the dynamic stall phenomenon for various angle-of-attack rates. As shown, rapid change in angle of attack causes separation and reattachment to be delayed, as governed by Eq. (11). The combination of the nonlinear static aerodynamics and the dynamic stall effects constitutes the aerodynamic model used throughout this study.

C. Optimization Problem Formulation

The trajectory optimization problem is formulated as a two-point boundary value problem between a cruising state and a perching state at a specified point. The final state is further restricted to have a pitch angle between 0–90 deg so that the aircraft could perch on its landing struts. For this study, a cost function is chosen to minimize the spatial bounds of the trajectory. With a thrust-to-weight ratio less than 1, the trajectory invariably "undershoots" the landing site because an increase in potential energy is required to reduce the speed to zero. Thus, the cost function addresses two major concerns: minimizing the undershoot and minimizing the distance from the landing site required to start the maneuver. Both goals have great practical value. Minimizing the undershoot is important due to spatial limitations because the landing site may be close to or at ground level or may be obstructed by objects in the environment. Minimizing the required distance to start the maneuver is important because on-board sensors, such as charge-coupled device (CCD) cameras, radar, or infrared range finders, have a finite range at which they can accurately identify and track the landing site. Increasing these sensors' ranges generally means increasing their size and weight, thereby increasing the demands on the aircraft design.

The persistent undershoot in the trajectories at low thrust-to-weight ratios motivates the division of the problem into two halves. Previous work has considered optimizing the entire trajectory at once for a mixed cost function that included undershoot and starting distance [21]. For this study, the goal of minimizing undershoot is given higher priority; thus, the problem can be divided and solved sequentially. These two halves, called the dive phase and the climb phase, are depicted in Fig. 7. The climb phase can be solved first for minimum undershoot by integrating the equations of motion [Eqs. (1–7)] from the lowest point of the trajectory (where $\gamma = 0$ deg) to the landing site. Previous studies [21] have shown that allowing a slightly positive final velocity decreases the required undershoot and removes the requirement that the aircraft be flying vertically before landing. The final velocity is specified to be 5% of the initial velocity, and the goal is to minimize the change in height between the initial and final points of the trajectory. The global (over all possible trajectories) minimum undershoot is a function only of the climb phase because only the dynamics here determine how quickly the aircraft can pull up to the landing site with the specified final speed. The dive phase then connects the initial condition to the starting point of the climb phase. This proposition assumes that the initial condition of the climb phase is a reachable end condition of the dive phase. The objective of the dive phase is to minimize the starting distance, which could be specified as horizontal, vertical, or Euclidean, for example, required to attain a final condition that matches the initial condition of the climb phase, which is stipulated to be the aircraft's straight and level trim point for maximum endurance.

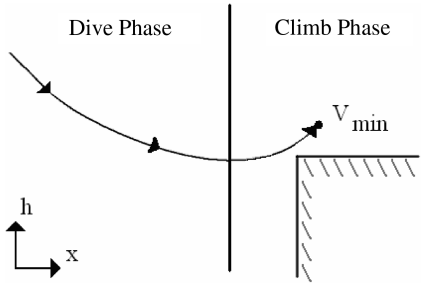

Fig. 7 Division of the perching trajectory optimization problem into two phases.

Thus, the cost functions for the two phases can be written as

$$J_{\text{dive}} = |x_f - x_i| \quad \text{or} \quad |h_f - h_i| \quad \text{or} \quad \sqrt{(x_f - x_i)^2 + (h_f - h_i)^2} \tag{15}$$

$$J_{\text{climb}} = -\min_{t\in[t_0,t_f]} h(t) \tag{16}$$

The requirement to minimize maximum undershoot [Eq. (16)] determines the optimal trajectory for the climb phase, which in turn determines the end condition of the dive phase. Thus, the optimal solution for the dive phase is only optimal among the set of trajectories that match up with the optimal trajectory for the climb phase. Although the solution to the dive phase may be suboptimal over all possible trajectories, it is optimal given the constraint that minimizing the maximum undershoot is the highest priority. Thus, the computed optimal trajectory minimizes the undershoot over all possible trajectories and minimizes the starting distance over all trajectories that minimize the undershoot.

III. Optimization Results

A. Conventional Aircraft

Although the point-mass aircraft problem described in [21] provides an adequate picture of the qualitative behavior of the perching problem, the bounds of the computed trajectories (i.e., the undershoot and the starting distance) are unrealistically small. This is due to the fact that the aircraft can pitch as fast as necessary to optimize the trajectory, without regard to rotational inertia or actuator limits. With the addition of the pitch dynamics governed by Eqs. (3) and (4), the pitch rate is now limited by the maximum achievable pitch moment and scaled by the rotational inertia of the aircraft. The pitch moment coefficient C_M in Eq. (3) is a function of the aircraft's angle of attack and the state of its geometry, determined by the actuators listed in Table 1. There is an additional pitch damping term C_{M_q}, proportional to the pitch rate q, that effectively smooths out rapid changes in pitch angle. Although this is desirable for gust alleviation, it is undesirable for maneuvers because the aircraft must produce a greater moment from its control surfaces to achieve rapid changes in pitch.

The maximum thrust-to-weight ratio is the first constraint to be varied because it has a large impact on the engine size and ultimately the power required for long endurance flight. These variations are depicted in Figs. 8 and 9, alongside a representative result from the point-mass analysis of [21]. As expected, a higher thrust-to-weight ratio permits lower undershoot. Physically, this seems counter-intuitive, after all, the objective is to minimize the kinetic energy of

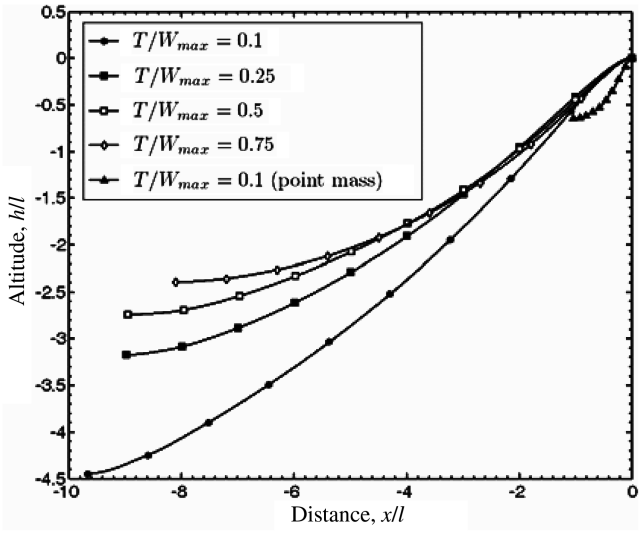

Fig. 8 Climb phase trajectories of varying maximum thrust-to-weight ratio.

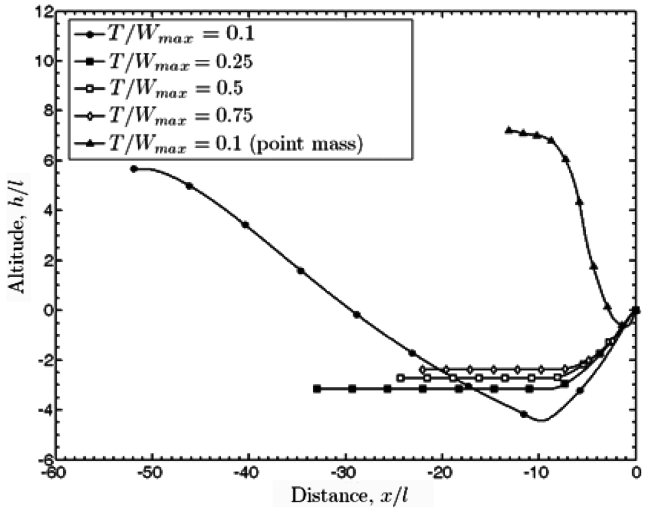

Fig. 9 Full trajectories of varying maximum thrust-to-weight ratio.

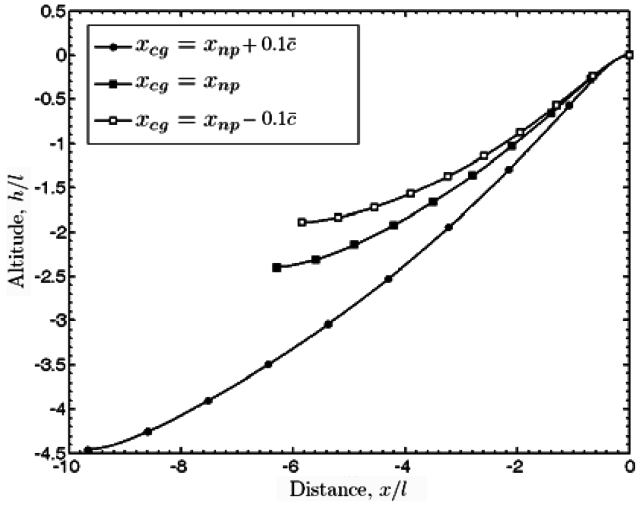

Fig. 11 Climb phase trajectories of varying center of gravity location ($T/W_{\max} = 0.1$).

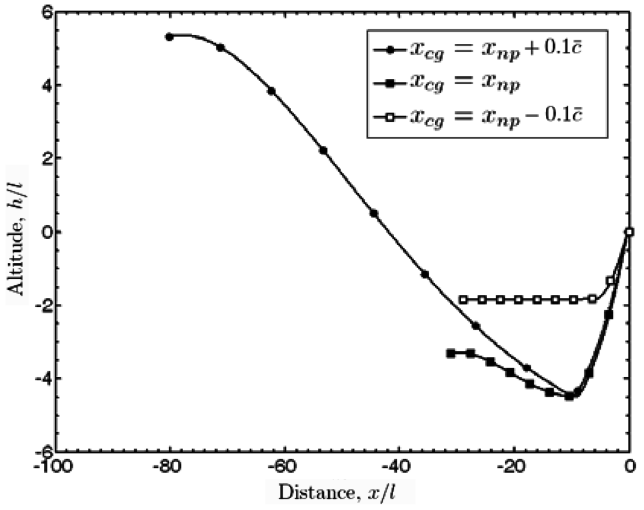

Fig. 12 Full trajectories of varying center of gravity location ($T/W_{\max} = 0.1$).

the system, whereas thrust can only increase it, but additional thrust allows the aircraft to fly at a slower speed while still climbing because the thrust line is not aligned with the velocity vector at nonzero angles of attack. Thus, the additional work done on the aircraft by the component of thrust along the trajectory is more than offset by the reduction in the required initial velocity (i.e., kinetic energy).

Complete trajectories of various maximum thrust-to-weight ratios are shown in Fig. 9. The dive phase for each variation is adjoined to its corresponding climb phase, with the end of each climb phase set to (0, 0). For each thrust-to-weight ratio, the dive phase is optimized for minimum altitude necessary to reach the required velocity at the start of the climb phase. For the cases in which this ratio is greater than 0.1, this altitude is zero (with respect to the start of the climb phase) because, with this much available thrust, the aircraft can trim at the required velocity for the climb. Below 0.25, diving is required to gain the kinetic energy needed to start the climb. Figure 10 indicates that maximum thrust is applied throughout the entire maneuver in the $T/W_{\max} = 0.1$ case, and, in the other cases, it is only used toward the end of the maneuver, when the aircraft is climbing. The thrust is also throttled right before landing, causing the aircraft to pitch down so that its final velocity is purely horizontal. The effects of the pitch dynamics can be seen by comparing the trajectories in Figs. 8 and 9 against the point-mass case. As predicted, the trajectories bear the same qualitative shape with much larger spatial bounds. Because the aircraft cannot pitch up as rapidly, it requires significantly more distance in which to complete the climb phase. Thus, although illustrative, a point-mass aircraft assumption does not capture the key physics of this problem.

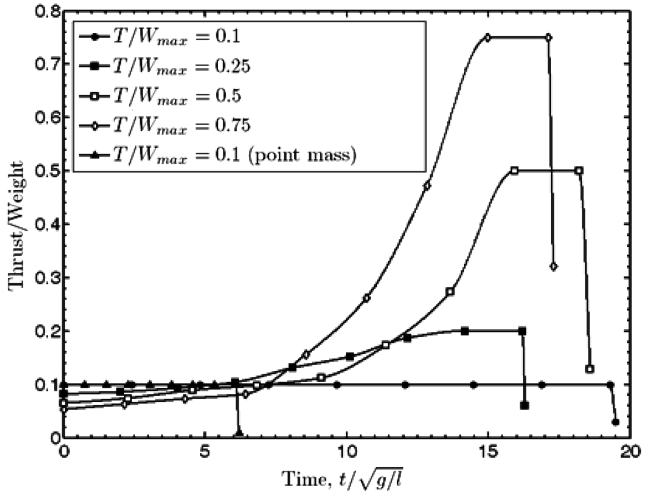

Fig. 10 Thrust-to-weight ratios vs time for full trajectories of varying maximum thrust-to-weight ratio.

In Figs. 11 and 12, maximum thrust-to-weight ratio is held constant, whereas the center of gravity position is varied with respect to the aircraft's neutral point. These plots indicate that the unstable aircraft ($x_{\text{cp}} = x_{\text{np}} - 0.1\bar{c}$) has a lower-cost (i.e., spatially smaller) optimal trajectory than the neutrally stable and stable aircraft. Because the unstable aircraft naturally pitches up when perturbed nose up from its equilibrium, it is able to pitch faster with less elevator deflection. This means the unstable aircraft can generate the same moment at lower speeds compared with the other aircraft; thus, it is able to fly slower and still climb to complete the maneuver. This lower flight speed requirement translates directly into smaller spatial bounds of the trajectory; hence, the aircraft's relative pitch stability plays a major role in its perching capability.

B. Morphing Aircraft

In-flight morphing allows the aircraft's dynamics to approach the point-mass case much more closely by enabling much larger possible pitching moments. This is because the morphing actuator ranges are much larger than the elevator's, as listed in Table 1; therefore, the lifting surfaces are able to rotate to higher angles of attack to generate larger pitching moments. By comparing the climb phase trajectories in Figs. 11 and 13, the direct results of these greater pitching moments can be seen by noting the reduced undershoot in the

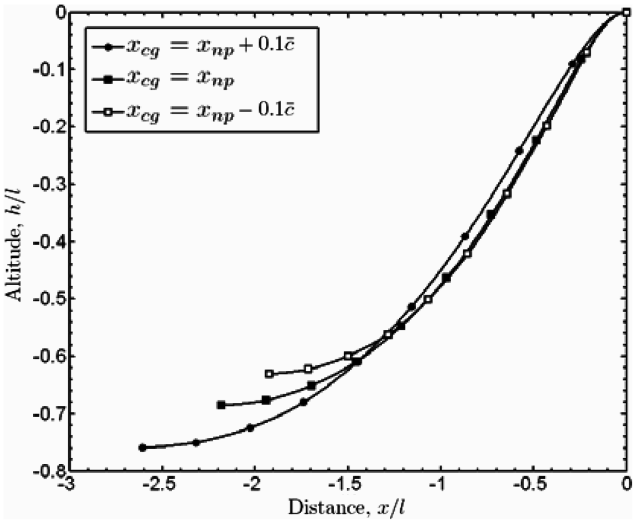

Fig. 13 Climb phase trajectories of varying center of gravity location for the aircraft with morphing ($T/W_{\max} = 0.1$).

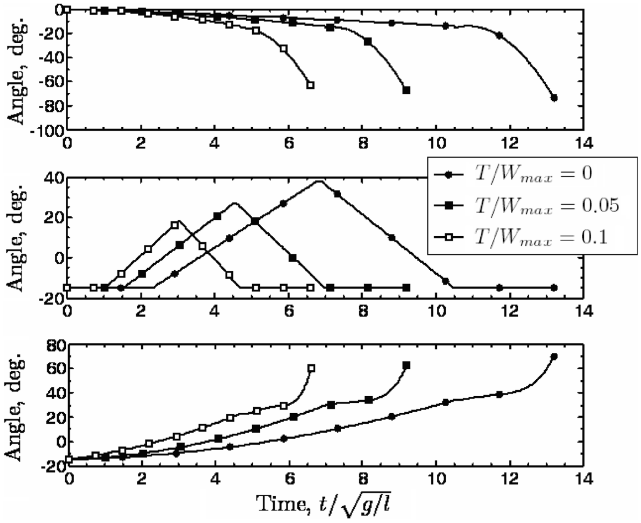

Fig. 15 Morphing parameter time histories of varying maximum thrust-to-weight ratio: wing incidence (top), tail boom angle (middle), and tail incidence (bottom).

morphing case. The morphing actuators are able to generate a larger moment at a lower speed, similar to the unstable aircraft discussed in the previous subsection. Because, for the morphing aircraft, the wings are not generating a large moment due to drag, their position with respect to the center of gravity is less significant compared with the tail's position. Thus, the morphing aircraft is less sensitive to changes in the center of gravity location compared with the fixed-configuration case of the previous subsection, as seen by comparing Figs. 11 and 13. Figures 14 and 15 show full trajectories of the morphing aircraft with varying thrust-to-weight ratios. For the dive phase, the aircraft must morph from its cruise configuration to the configuration in which it begins the climb phase over the shortest distance. As previously discussed, additional thrust enables the aircraft to fly at much lower speeds, thereby shortening this distance. Figure 15 depicts the time histories of the morphing parameters for these trajectories. In these simulations, the elevator deflection is held at zero to isolate the effects of vehicle reconfiguration. The wing incidence time history indicates that the wings should be pitched down as the fuselage pitches up, thereby maintaining attached flow over the wings throughout the maneuver. This is beneficial for maintaining aileron effectiveness and for maximizing the pitching moment contribution of the wings. The wing incidence and tail incidence increase monotonically over this phase, indicating a transition from one trim state at cruise to another at the bottom of the trajectory. The tail boom is swung down and then back up again, which serves to pitch the aircraft down to gain speed for the climb phase. During the climb phase, the tail boom remains fixed at its lower bound, which produces the largest moments due to down force and drag on the tail. The tail incidence angle is gradually increased, thereby producing a greater and greater negative tail angle of attack. At first, this produces a large downforce on the tail, pitching the aircraft up. As the aircraft approaches the landing site, the angle of attack decreases further, thereby increasing the drag and slowing and pitching down the aircraft. Figure 16 presents a direct comparison between a fixed configuration and a morphing aircraft of the same thrust-to-weight ratio, indicating the orientation of the aircraft at several points along the trajectory. It is apparent that morphing helps increase the maneuverability of the aircraft, thus enabling it to perch within a much shorter distance.

Finally, the controllability of the aircraft during the perching maneuver is studied. Specifically, the effectiveness of the elevators is discussed because the aircraft is only simulated in the longitudinal plane. Figure 17 depicts the maximum change in pitching moment coefficient from the nominal along the trajectory due to elevator deflection in the upward and downward directions from its trimmed position. Thus, this plot represents the additional control authority, useful for disturbance rejection, for example, available throughout

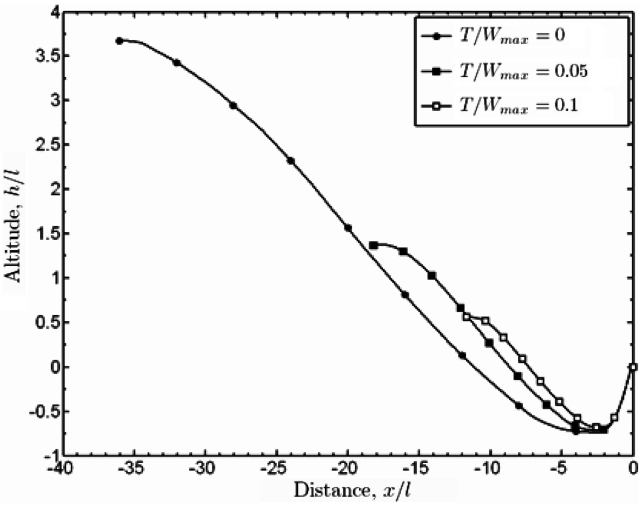

Fig. 14 Full trajectories of varying maximum thrust-to-weight ratio for the aircraft with morphing.

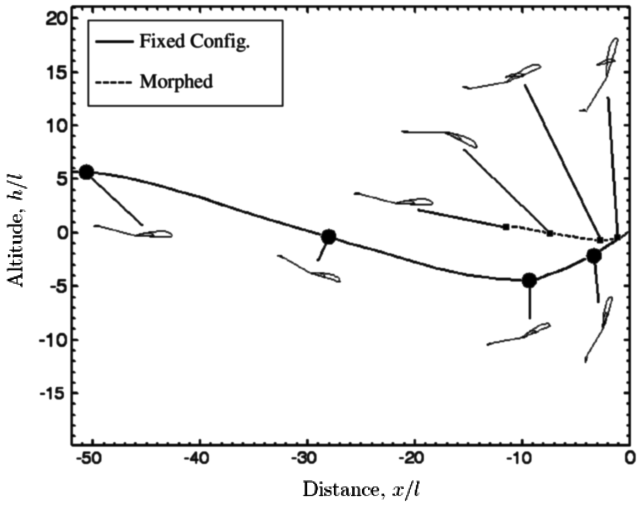

Fig. 16 Comparison of fixed-configuration and morphing aircraft perching trajectories ($T/W_{\max} = 0.1$).

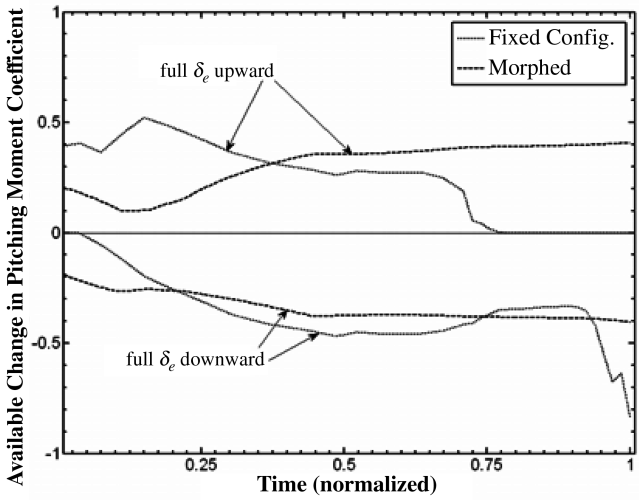

Fig. 17 Elevator effectiveness for fixed-configuration and morphing aircraft.

the maneuver. In Fig. 17, the cases in which the maximum thrust-to-weight ratio is 0.1 and the center of gravity is located at the neutral point are compared between morphing and fixed-configuration aircraft. Because these two maneuvers have different durations, time is normalized from 0 to 1, representing the beginning and the end of the maneuvers, respectively. In general, the morphed case maintains high control authority in both directions (i.e., pitch up and pitch down) throughout the maneuver. At the beginning and at the end of the maneuver, the fixed-configuration case only has authority in one direction because the elevators are fully deflected to track the optimal trajectory. The morphed case becomes worse around 15% of the way through the maneuver because the tail boom is briefly rotating the elevators into the stalled regime to pitch the aircraft downward. This problem could be alleviated by factoring in controllability into the cost function as a future point of study. If a specified level of control authority is added as a constraint, then the elevator time history could be optimized along with the morphing degrees of freedom to improve the trajectory further while maintaining adequate disturbance rejection capability. Indeed, this flexibility is one of the hallmarks of adding additional morphing degrees of freedom to the airframe.

IV. Conclusions

The problem of designing a trajectory to perch a low thrust-to-weight aircraft on a platform has been formulated and solved for fixed-configuration and morphing airframes. These trajectories invariably feature an undershoot of the landing site due to the combination of low required landing speed and low thrust to weight. If this undershoot is to be minimized, then the trajectory can be effectively broken into two subproblems: a dive phase followed by a climb phase. The aircraft dynamics during the climb phase determine the undershoot of the trajectory, whereas the dive phase determines the starting distance of the maneuver. Because the aircraft must pitch up to high angles of attack to perch, pitch moment authority plays a key role in this optimization problem. The location of the center of gravity is a very important factor in determining the cost of the optimal trajectory because it has a direct effect on the pitch stiffness of the aircraft. In fact, pitch instability improves the perching trajectories in the sense of reducing their spatial bounds over stable airframes. Furthermore, the addition of a few judicious morphing degrees of freedom improves the optimal perching trajectory by adding a much larger pitching moment capability. Through morphing, the effectiveness of the control surfaces increases throughout the maneuver because they are maintained at low angles of attack and not used in the maneuver itself. Thus, morphing is effective at increasing the open- and closed-loop capabilities of the aircraft during the perching maneuver.

Acknowledgments

This work is supported by the Defense Advanced Research Projects Agency (DARPA) and the Army Research Office (ARO), contract 48730-EG-DRP, under program manager Darryll Pines. It is also supported by the NASA Langley Research Center through the Graduate Student Research Program grant number NGT-1-03022. This grant is monitored by Martin Waszak and Anna-Maria McGowan. The authors also acknowledge the support of the American Society for Engineering Education (ASEE) Summer Faculty Fellowship Program for funding research conducted at Wright–Patterson Air Force Base under the advisement of Brian Sanders during the summer of 2006.

References

[1] Sanders, B., Crowe, R., and Garcia, E., "Defense Advanced Research Projects Agency: Smart Materials and Structures Demonstration Program Overview," *Journal of Intelligent Material Systems and Structures*, Vol. 15, No. 4, 2004, pp. 227–233. doi:10.1177/1045389X04042793

[2] Bowman, J., Sanders, B., and Weisshaar, T., "Evaluating the Impact of Morphing Technologies on Aircraft Performance," AIAA Paper 2002-1631, 2002.

[3] Wickenheiser, A., Garcia, E., and Waszak, M., "Evaluation of Bio-Inspired Morphing Concepts with Regard to Aircraft Dynamics and Performance," *Proceedings of SPIE: International Society for Optical Engineering*, Vol. 5390, July 2004, pp. 202–211. doi:10.1117/12.540346

[4] Tidwell, Z., Joshi, S., Crossley, W. A., and Ramakrishnan, S., "Comparison of Morphing Wing Strategies Based Upon Aircraft Performance Impacts," AIAA Paper 2004-1722, 2004.

[5] Bye, D. R., and McClure, P. D., "Design of a Morphing Vehicle," AIAA Paper 2007-1728, 2007.

[6] Flanagan, J. S., Strutzenberg, R. C., Myers, R. B., and Rodrian, J. E., "Development and Flight Testing of a Morphing Aircraft, the NextGen MFX-1," AIAA Paper 2007-1707, 2007.

[7] DeLaurier, J. D., "The Development and Testing of a Full-Scale Piloted Ornithopter," *Canadian Aeronautics and Space Journal*, Vol. 45, No. 2, 1999, pp. 72–82.

[8] Taylor, G. K., Bomphrey, R. J., and 't Hoen, J., "Insect Flight Dynamics and Control," AIAA Paper 2006-32, 2006.

[9] Tobalske, B. W., Warrick, D. R., Clark, C. J., Powers, D. R., Hedrick, T. L., Hyder, G. A., and Biewener, A. A., "Three-Dimensional Kinematics of Hummingbird Flight," *Journal of Experimental Biology*, Vol. 210, No. 18, 2007, pp. 3135–3146. doi:10.1242/jeb.000273

[10] Wang, Z. J., "Dissecting Insect Flight," *Annual Review of Fluid Mechanics*, Vol. 37, No. 1, 2005, pp. 183–210. doi:10.1146/annurev.fluid.36.050802.121940

[11] Wickenheiser, A., Garcia, E., and Waszak, M., "Longitudinal Dynamics of a Perching Aircraft Concept," *Proceedings of SPIE: International Society for Optical Engineering*, Vol. 5764, May 2005, pp. 192–202. doi:10.1117/12.601512

[12] Wickenheiser, A., and Garcia, E., "Longitudinal Dynamics of a Perching Aircraft," *Journal of Aircraft*, Vol. 43, No. 5, 2006, pp. 1386–1392. doi:10.2514/1.20197

[13] McGahan, J., "Gliding Flight of the Andean Condor in Nature," *Journal of Experimental Biology*, Vol. 58, No. 1, 1973, pp. 225–237.

[14] Crowther, W. J., "Perched Landing and Takeoff for Fixed Wing UAVs," *NATO Symposium on Unmanned Vehicles for Aerial, Ground, and Naval Military Operations*, 2000.

[15] Levine, J. S., Blaney, D. L., Connerney, J. E. P., Greeley, R., Head, J. W., Hoffman, J. H., Jakosky, B. M., McKay, C. P., Sotin, C., and Summers, M. E., "Science from a Mars Airplane: The Aerial Regional-Scale Environmental Survey (ARES) of Mars," AIAA Paper 2003-6576, 2003.

[16] Enright, P. J., and Conway, B. A., "Discrete Approximations to Optimal Trajectories Using Direct Transcription and Nonlinear Programming," *Journal of Guidance, Control, and Dynamics*, Vol. 15, No. 4, 1992, pp. 994–1002.

[17] Fritsch, F. N., and Carlson, R. E., "Monotone Piecewise Cubic Interpolation," *SIAM Journal on Numerical Analysis*, Vol. 17, No. 2, 1980, pp. 238–246. doi:10.1137/0717021

[18] Atiqullah, M. M., "Tuned Annealing for Optimization," *Computational*

Science, Vol. 2074, Lecture Notes in Computer Science, Springer, Berlin, 2001, pp. 669–679.

[19] Powell, M. J. D., "A Fast Algorithm for Nonlinearly Constrained Optimization Calculations," *Numerical Analysis*, edited by G. A. Watson, Lecture Notes in Mathematics, Vol. 630, Springer–Verlag, New York, 1978, pp. 144–157.

[20] Dormand, J. R., and Prince, P. J., "A Family of Embedded Runge–Kutta Formulae," *Journal of Computational and Applied Mathematics*, Vol. 6, No. 1, 1980, pp. 19–26. doi:10.1016/0771-050X(80)90013-3

[21] Wickenheiser, A., and Garcia, E., "Perching Aerodynamics and Trajectory Optimization," *Proceedings of SPIE: International Society for Optical Engineering*, Vol. 6525, 65250O, April 2007. doi:10.1117/12.716069

[22] Stengel, R. F., *Optimal Control and Estimation*, Dover, Mineola, NY, 1994, pp. 421–432.

[23] Betts, J. T., *Practical Methods for Optimal Control Using Nonlinear Programming*, SIAM, Philadelphia, PA, 2001, Chap. 1.

[24] Weissinger, J., "The Lift Distribution of Swept-Back Wings," NACA TM-1120, 1947.

[25] Wickenheiser, A., and Garcia, E., "Aerodynamic Modeling of Morphing Wings Using an Extended Lifting-Line Analysis," *Journal of Aircraft*, Vol. 44, No. 1, 2007, pp. 10–16. doi:10.2514/1.18323

[26] Sheldahl, R. E., and Klimas, P. C., "Aerodynamic Characteristics of Seven Symmetrical Airfoil Sections through 180-Degree Angle of Attack for Use in Aerodynamic Analysis of Vertical Axis Wind Turbines," Sandia National Laboratories Rept. SAND80-2114, 1981.

[27] Goman, M., and Khrabrov, A., "State-Space Representation of Aerodynamic Characteristics of an Aircraft at High Angles of Attack," *Journal of Aircraft*, Vol. 31, No. 5, 1994, pp. 1109–1115.